

Conformal and Nanoscale Poly(pyrrole) Coating on Li_3VO_4 Surface Enabling High Performance Lithium-Ion Batteries

Mini Pothanadu Antony, Dona Susan Baji, Shantikumar Nair,
and Dhamodaran Santhanagopalan*

Lithium vanadium oxide (Li_3VO_4) shows great promise as an anode for high-efficiency Li-ion batteries (LIBs). However, its application is hindered by poor electronic conductivity and high charge transfer resistance caused by a thick and unstable solid electrolyte interface layer. A two-step approach aimed at improving the electrochemical performance of the LVO anode for high-rate and long-cycle LIBs is reported. This involves the hydrothermal synthesis of crystalline LVO, followed by a conformal coating of polypyrrole (Ppy) via vapor-phase polymerization. The conductive Ppy layer facilitates electron transport and enhances lithium-ion diffusion, mitigating the limitations of pristine LVO. Among the tested samples, LVO@Ppy-0.5 (0.5

indicates coating time in hours) exhibited the highest reversible capacity of 605 mAh g^{-1} , nearly three times that of pristine LVO with an initial Coulombic efficiency of 87% upon chemical pre-lithiation. The rate capability studies revealed stable performance, with 78% capacity retention over 500 cycles at 10C. Electrochemical impedance spectroscopy reveals that the LVO@Ppy-0.5 electrode exhibits high Li-ion diffusivity, reduced interfacial layer resistance, and enhanced charge transfer kinetics. Ex situ surface chemical analysis confirms the formation of a stable solid-electrolyte interphase layer on LVO@Ppy-0.5. Conformal Ppy coating on LVO is a promising strategy for developing high-performance LIB anode.

1. Introduction

Fossil fuels are nonrenewable, underscoring the importance of developing ecofriendly, replenishable, and long-lasting energy sources like wind and solar.^[1,2] However, the intermittent nature of renewable energy sources, combined with the escalating demand for applications like electric vehicles (EVs), has highlighted the need for efficient energy storage technologies, such as, lithium-ion batteries (LIBs). Despite their advantages, current LIBs cannot meet the increasing demands of next-generation EVs and hybrid vehicles, which require batteries with enhanced rate capability, significantly higher capacity, longer cycle life, and excellent safety profiles.^[3] The next generation of LIBs needs improvements in power densities, safety, cost, and cycle life. Graphite has been widely adopted as a commercial LIB anode material due to its promising advantages, however at high rates, low operational voltage leads to dendrite growth and holds safety concerns.^[4,5] $\text{Li}_4\text{Ti}_5\text{O}_{12}$ (LTO) is also widely researched as a zero-strain anode material because of its stable intercalation process without significant volume changes. Nevertheless, the

cell voltage and total energy density are compromised by LTO's lower theoretical capacity ($\approx 150 \text{ mAh g}^{-1}$) and higher voltage platform ($\approx 1.6 \text{ V vs. Li/Li}^+$).^[6–8] To improve performance and address the aforementioned problems of LIBs, it is imperative to design appropriate anode materials. Lithium vanadium oxide (Li_3VO_4 , LVO) has garnered interest as an advanced anode material for LIBs, owing to its cost-effectiveness, relatively high theoretical capacity ($\approx 394 \text{ mAh g}^{-1}$), and stable discharge plateau.^[9] Its redox potential is lower than that of LTO and higher than graphite, increasing energy density and reducing the risk of short circuits caused by lithium dendrite formation.^[9] LVO provides a higher reversible capacity than graphite and LTO, along with improved safety.^[10] It exhibits high Li^+ ionic mobility ($\approx 10^{-4}$ to 10^{-6} S m^{-1}),^[11] and minimal morphological and volumetric changes (4%) in the course of the lithiation/delithiation process.^[12] The crystal structure of Li_3VO_4 , consisting of corner-shared VO_4 and LiO_4 tetrahedrons, facilitates the intercalation of lithium ions into vacancies, leading to minimal volume changes during charge and discharge cycles. Despite its potential, Li_3VO_4 encounters several challenges, including limited and unstable reversible capacities, low initial Coulombic efficiencies, and significant polarization. These issues are primarily attributed to its poor electrical conductivity and sluggish lithium-ion diffusion.^[13]

Various strategies have been explored to enhance the electrical conductance and the coefficient of diffusion of Li_3VO_4 , including synthesizing materials with different structures, metal ion doping, coating with carbon or other conductive materials, compositing, and minimizing particle size to the nanometer scale.^[14,15] These techniques have enhanced electrochemical characteristics like discharge capacity, rate capability, and cycle stability by shortening the transport distances for both electrons

M. Pothanadu Antony, D. S. Baji, S. Nair, D. Santhanagopalan
Amrita School of Nanosciences and Molecular Medicine

Amrita Vishwa Vidyapeetham

Kochi 682041, India

E-mail: dsgopalan20710@aims.amrita.edu

M. Pothanadu Antony

Department of Physics

St. Michael's College

Cherthala 688539, India

 Supporting information for this article is available on the WWW under <https://doi.org/10.1002/batt.202500575>

and lithium ions. According to a recent report, the Li_3VO_4 -based electrode can achieve unprecedented high-rate performance through a novel honeycomb architecture and electrochemical reconstruction upon cycling.^[16] Furthermore, surface coating is a crucial modification technique since it can significantly improve the electrode materials' electrical conductivity, thermal stability, cycle life, and a variety of other physico-chemical and electrochemical properties.^[16–24] Several coatings were implemented to address the limitations of Li_3VO_4 .^[16] and these coating materials include carbon, modified carbon, graphene, polymers, and others that significantly improve the electronic conductivity of Li_3VO_4 . This enhancement minimizes polarization, helps to accommodate volume changes during lithiation/delithiation reactions, and reduces structural damage to Li_3VO_4 . Additionally, surface coating with conducting polymers is an efficient way to enhance electrochemical properties as the polymers have high conductivity.^[18] As per the literature, the 2D structure of LVO@NC nanosheets ensures excellent reaction activity and rate performance. They deliver 628.4 mAh g⁻¹ after 300 cycles at 0.2 A g⁻¹ and retain 610.3 mAh g⁻¹ after 460 cycles, showing great potential for high-power lithium-ion batteries.^[19]

Conducting polymers, such as polythiophene (PTH), polyaniline (PANI), polyparaphhenylene (PPP), polyphenylenevinylene (PPV) and polypyrrole (Ppy), are particularly appealing due to their unique metallic/seiconductor properties, high charge density, cost-effectiveness, and excellent electronic properties. Polypyrrole (Ppy) is a well-studied conducting polymer, recognized for its simple and cost-effective synthesis, exceptional electrical conductivity, and stability in both chemical and electrochemical environments.^[20–22] Hsu et al.^[17] reported that a uniform PEDOT coating on LVO improves the initial Coulombic efficiency (ICE) by enhancing the electronic conductivity of Li_3VO_4 and protecting it from corrosion and dissolution in the electrolyte during charge/discharge cycles. The polymer layer serves as a stable interface between Li_3VO_4 and the electrolyte. Sun and colleagues^[23] reported that a thin Ppy coating enhances both electronic conductivity and structural integrity, thereby improving the overall performance of zinc ferrite hollow spheres. PEDOT:PSS-coated Co_3O_4 anode delivered improved the sodium ion storage performance compared to the pristine anode material.^[24]

In this study, a two-step process of hydrothermal synthesis followed by a vapor phase polymerization was utilized to synthesize polypyrrole-coated LVO (LVO@Ppy). Beyond enhancing conductivity, the polymer matrix can buffer the $\approx 4\%$ volume change of LVO during cycling, thereby improving structural integrity. The electrochemical nature of the as-prepared LVO and Ppy-decorated LVO was thoroughly analyzed. The vapor-phase polymerization enables conformal and controllable coatings over LVO, ensuring uniform coverage. The best charge capacity achieved is 605 mAh g⁻¹ at a rate of C/2 within a broader electrochemical window of 0.01–3.0 V. Comprehensive cycling stability and rate studies were also conducted. The Ppy-decorated LVO anode demonstrated outstanding cycling performance and rate capability, attributed to the increased conductivity offered by the Ppy coating. Additionally, the Ppy coating acted as a protective shield between the active material LVO and the corrosive electrolyte.

2. Experimental Section

2.1. Hydrothermal Synthesis of LVO

Ammonium metavanadate (NH_4VO_3) (SRL, India) and lithium hydroxide (LiOH) (Sigma Aldrich) were each dissolved separately in deionized water at a 1:3 molar ratio. The solutions were then combined in a steel autoclave lined with Teflon, where the hydrothermal process was performed at 180 °C for 24 h. Following centrifugation, the product was washed with deionized water and ethanol, yielding a white powder, which was designated as LVO.

2.2. Ex Situ Vapor Phase Polymerization of Pyrrole on LVO

A simple and cost-effective vapor-phase polymerization technique was employed to deposit Ppy on LVO. Initially, 150 mg of LVO was soaked in 0.1 mL of FeCl_3 oxidant solution (0.3 M) and dried overnight. For the polymerization process, a vial containing 2 mL of pyrrole monomer and a second vial containing 150 mg of FeCl_3 -soaked LVO were sealed inside a Borosil TM bottle and maintained at 50 °C for varying durations (Figure 1). Due to the low vapor pressure of pyrrole, its molecules evaporated and diffused to the exterior of the LVO particles. In the presence of the FeCl_3 , the pyrrole monomers underwent polymerization on the LVO surface, forming LVO@Ppy.^[22] The polymerization durations were 0.5, 1, 2.5, and 5 h, and the corresponding samples were labeled as LVO@Ppy-0.5, LVO@Ppy-1.0, LVO@Ppy-2.5, and LVO@Ppy-5.0, respectively.

2.3. Material Characterizations

The crystal structure and phase purity of pristine LVO and LVO@Ppy were examined using X-ray diffraction analysis (XRD: D2 Phaser, Bruker), with Cu K_α radiation used to characterize the samples. Morphological analysis was done using field emission scanning electron microscopy (FESEM, Jeol, Japan). Transmission electron microscopy (TEM), images were obtained to verify the Ppy coating over LVO. Thermal gravimetric analysis (TGA) was used to study thermal stability and the weight ratio of Ppy on LVO@Ppy, at a heating ramp of 10 °C min⁻¹ from 25 to 700 °C. Surface chemical evaluation was conducted with X-ray photoelectron spectroscopy (XPS, Kratos, Axis Ultra, UK) using an Al K_α X-ray source. Fourier transform infrared spectroscopy (FTIR) was recorded using Nicolet FTIR Spectrometer (Thermo Fischer Scientific, India), in the wavenumber range from 4000 cm⁻¹ to 400 cm⁻¹ and with a 0.5 cm⁻¹ step size.

2.4. Electrochemical Characterizations

The electrochemical properties of Pristine LVO and LVO@Ppy electrodes were evaluated using galvanostatic charge-discharge (GCD) measurements at various C rates, with a cut-off voltage set between 0.01 and 3.0 V versus Li/Li⁺. The slurry was prepared with 75 wt% active material, 15 wt% multiwalled carbon nanotubes (MWCNT) (Reinstet, India) as conducting additive and 10 wt% polyvinylidene fluoride (PVDF) as the binder. The composites were

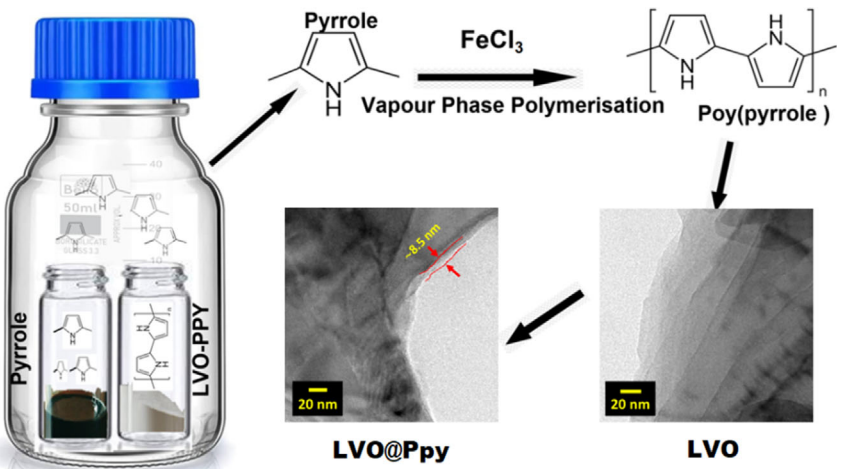


Figure 1. Schematic representation of vapor phase polymerization of Poly(pyrrole) on LVO.

thoroughly mixed with N-methyl-2-pyrrolidone (NMP) and the slurry was applied onto the Cu foil by the doctor blading technique. All samples were subsequently dried in an IR lamp oven at 120 °C for 15–30 min. After drying and pressing, the electrodes were cut into 1.0 cm² circular discs, with electrode loadings typically maintained between 1 and 1.35 mg cm⁻². The cells were then assembled inside glove box, which maintained the moisture and O₂ level below 1 ppm (Mbraun, Germany). One widely adopted prelithiation approach involves immersing the electrode in a lithium–aromatic–ether solution, which enables effective lithium-ion insertion into the active material. In this study, lithium biphenyl (Li-Bp) was used for the prelithiation process. The LVO@Ppy-0.5 anodes were immersed in a 3 M Li-Bp solution in 2-methyltetrahydrofuran (2-MeTHF) for 1 min, followed by quenching.^[25] The electrochemical analysis was carried out in Swagelok-type cells with two-electrodes, with lithium foil acting as both the counter and reference electrodes. The electrolyte was prepared as a 1 M LiPF₆ solution in a 1:1 volume ratio mixture of ethylene carbonate (EC) and dimethyl carbonate (DMC) (PURIEL, Canada), and glass microfiber was utilized as separator. Material analysis and electrochemical analysis were carried out using a Bio-Logic instrument by assembling half-cells with a voltage window of 0.01–3.0 V. Electrochemical impedance spectroscopy (EIS) was conducted using a 50 mV AC amplitude within a frequency range of 10 kHz to 10 mHz.

2.5. Ex Situ XPS Analysis

Ex situ XPS measurements were performed on electrodes at various stages of lithiation and delithiation in a half-cell configuration during the first cycle, which was conducted at 1C rate within a voltage range of 0.01–3.0 V. The electrodes analyzed included pristine LVO (pristine), LVO at the end of the first discharge to 0.01 V, and LVO at the end of the first cycle (discharge to 0.01 V followed by charge to 3.0 V). Similarly, LVO@Ppy-0.5 electrodes were examined in their pristine state, after the first discharge to 0.01 V, and after completion of the first cycle (discharge to

0.01 V and subsequent charge to 3.0 V). Following this, the cells were carefully disassembled inside a glove box maintained at O₂ and H₂O levels below 1.0 ppm. The electrodes were then rinsed with dimethyl carbonate to remove residual salts and allowed to dry inside the glove box. The prepared electrodes were placed in the XPS sample holder and transferred to the load-lock compartment with minimal exposure to ambient conditions. During data acquisition, charge neutralization was applied to minimize charging effects, and high-resolution spectra were recorded using a pass energy of 20 eV, averaging over five scans.

3. Results and Discussion

Figure 2 shows the XRD pattern of the as prepared LVO and LVO@Ppy samples. The XRD analysis reveals that the hydrothermal synthesis results in a highly crystalline, single-phase LVO with an orthorhombic structure (JCPDS No. 38-1247), with no need for further annealing. The XRD patterns of LVO@Ppy-0.5, LVO@Ppy-1.0, LVO@Ppy-2.5, and LVO@Ppy-5.0 remained nearly identical to

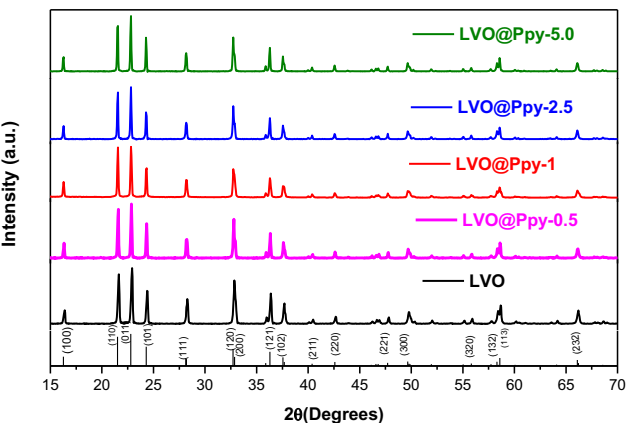


Figure 2. XRD spectra of pristine-LVO and LVO@Ppy samples.

that of the pristine LVO sample, implying that the coating process had no impact on the crystal structure of pristine LVO.

TGA in air was performed to determine the Ppy weight percentage (Figure S1, Supporting Information). The TGA curve for pristine LVO exhibits a weight loss of ≈ 0.7 wt% as the temperature increases to 700 °C. In contrast, the LVO@Ppy sample exhibits two distinct weight loss stages. A small weight loss below 100 °C is associated with the evaporation of moisture content, while a more substantial loss between 100 and 450 °C indicate the thermal decomposition of Ppy in air.^[23] According to TGA analysis, the Ppy weight percentages in LVO@Ppy are 1.68 wt%, 2.20 wt%, 2.26 wt%, and 2.37 wt% for LVO@Ppy-0.5, LVO@Ppy-1.0, LVO@Ppy-2.5, and LVO@Ppy-5.0, respectively (Table S1, Supporting Information). Figure S2, Supporting Information, shows the FTIR spectra of bare LVO and LVO@Ppy-0.5, confirming the formation of polypyrrole on the surface of LVO particles. Polypyrrole exhibits a broad band at 3440 cm⁻¹, corresponding to the N–H stretching vibration, while the band at 1630 cm⁻¹ originates from the C=C stretching mode of the pyrrole ring.^[26] These prominent peaks clearly indicate the presence of Ppy. The characteristic absorption bands of Li₃VO₄ are typically located in the range of 750–850 cm⁻¹; therefore, the band at 765 cm⁻¹ is attributed to the asymmetric stretching of VO₄³⁻ groups in LVO,^[27] which appears in both bare LVO and LVO@Ppy-0.5 samples. This confirms that the polymer coating does not alter the crystal structure of LVO.

The morphology of pristine LVO and LVO@Ppy samples are shown in FESEM images. Figure S3b–e, Supporting Information, displays the surface morphology of LVO@Ppy-0.5, LVO@Ppy-1.0, LVO@Ppy-2.5, and LVO@Ppy-5.0, respectively. As the polymerization time increases, the Ppy coating thickness on LVO increases. A 5-h process clearly results in a dense Ppy layer, while a 0.5-h

deposition yields only a thin Ppy coverage on the LVO surface. Figure 3 presents the TEM and High-resolution TEM (HRTEM) images of LVO, LVO@Ppy-1.0, and LVO@Ppy-5.0. Figure 3a–c displays the low magnification TEM images of the LVO, LVO@Ppy-1.0, and LVO@Ppy-5.0 samples, respectively. The Ppy coating was evidenced with a thickness of about 4.5 and 8.5 nm for LVO@Ppy-1.0 and LVO@Ppy-5.0, respectively, indicating increase of thickness consistent with the process time. Figure 3d–f indicates the HRTEM image of LVO, LVO@Ppy-1.0, and LVO@Ppy-5.0, respectively. The HRTEM images reveals that all the three samples exhibit lattice fringes spaced between 3.95 and 4.10 Å, corresponding to the (011) plane of Li₃VO₄.^[17] Figure 3e–f indicates that LVO@Ppy also exhibits a crystalline structure with lattice fringes spaced at 3.9 Å, identical to the pristine LVO. This suggests that the polymerization did not alter the interplanar spacing or the crystallinity of the host material. It is expected that the conductive Ppy layer can improve the electrical conductivity of the LVO, leading to percolated pathway for charge transport.

Elemental identification through energy-dispersive X-ray spectroscopy demonstrates that Carbon (C), Vanadium (V), and Oxygen (O), are present in the LVO particles (Figure S4, Supporting Information). The presence of Fe and Cl is attributed to the FeCl₃ used as polymerizing agent, while the presence of C and N confirms the formation of Ppy. The carbon content in LVO@Ppy is higher than that in the pristine LVO sample, likely due to the presence of Poly(pyrrole). As the time of polymerization increases the degree of polymerization and coating thickness increases as indicated by the weight loss and the TEM discussed earlier. However, the rate of increase appears to saturate for longer duration, indicating that the polymerization process might self-limit the coating thickness on the surface of LVO.

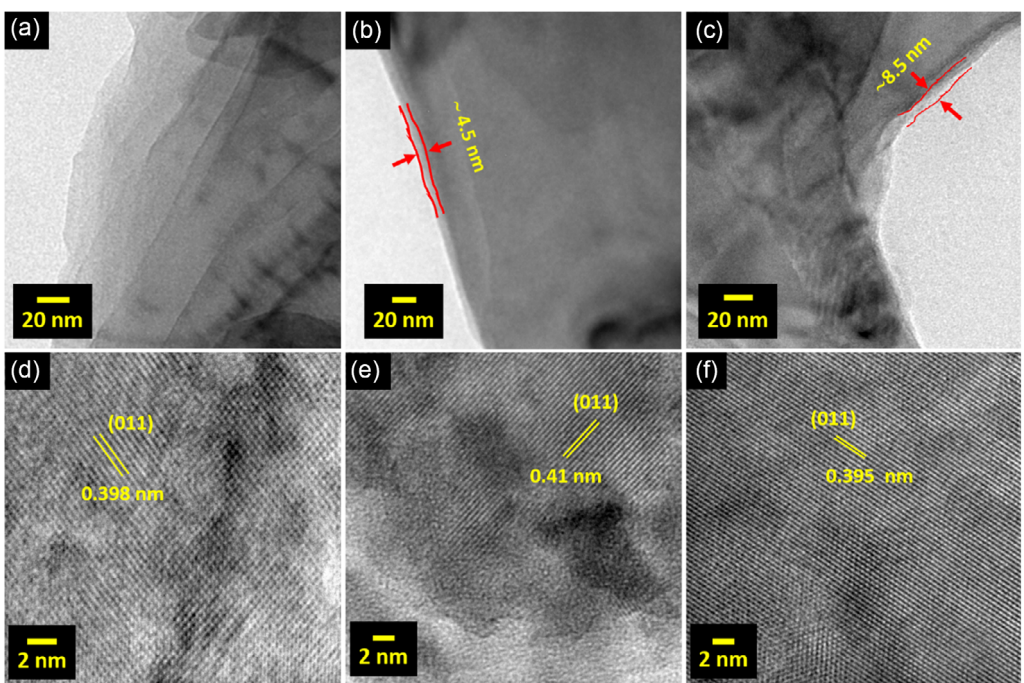


Figure 3. TEM images of a) pristine LVO, b) LVO@Ppy-1, and c) LVO@Ppy-5, and HRTEM images of d) pristine LVO, e) LVO@Ppy-1, and f) LVO@Ppy-5.

The valence states of the LVO and LVO@Ppy samples were analyzed using XPS. The survey spectrum in Figure S5, Supporting Information, shows that the materials are primarily composed of C 1s, O 1s Li 1s, and V 2p. The LVO@Ppy-5.0 sample shows additional peaks corresponding to N 1s, Fe 2p, and Cl 2p, with the Fe 2p and Cl 2p peaks originating from the oxidizing agent FeCl_3 . Figure 4 is the high resolution XPS, Figure 4a C 1s shows the C–C chemical state of 284.6 eV, C–N/C–O of 285.6 eV, and the chemical state of C=N/C=O of 287.9 eV coexist.^[28] Figure 4b displays peaks at 530.5 eV binding energy of O 1s. Figure 4c verifying the presence of the V–O bond in the LVO@Ppy samples of V 2p after fitting; the V^{5+} 2p_{3/2} and V^{5+} 2p_{1/2} peaks identified at 517.8 and 525.0 eV, respectively, which align with the values reported in literature.^[29,30] Additionally, peaks corresponding to the oxidation state of vanadium (4+) and are clearly identified at 516.8 (V^{4+} 2p_{3/2}) and 523.9 eV (V^{4+} 2p_{1/2}). Figure 4d displays peaks at 55 eV correspond

to the Li 1s and 530.5 eV verifying the presence of the V–O bond. The N 1s peak at 399.7 eV for LVO@Ppy-5.0 sample verifies the existence of C–N bond, which is consistent with the N 1s peak observed for Ppy.^[28]

The stabilized reversible specific capacity at different C-rates is detailed in Table S2, Supporting Information. From the charge capacity and rate performance study (Figure 5), among LVO@Ppy-0.5, LVO@Ppy-1.0, LVO@Ppy-2.5, and LVO@Ppy-5.0 samples, and the LVO@Ppy-0.5 anode achieved a maximum reversible charging capacity of 605 mAh g^{-1} . The rate capability of all the LVO and LVO@Ppy samples were conducted and depicted in Figure 5a. The test was carried from C/2, 1C, 2C, 5C, and C/2 (1C = 400 mA g^{-1}) with current densities ranging from 100 to 4000 mA g^{-1} . As the current density was increased, the charge capacity progressively declined (see Figure 5, Table S1, Supporting Information). After five cycles at varying current densities, the current was reverted to 100 mA g^{-1} , with nearly

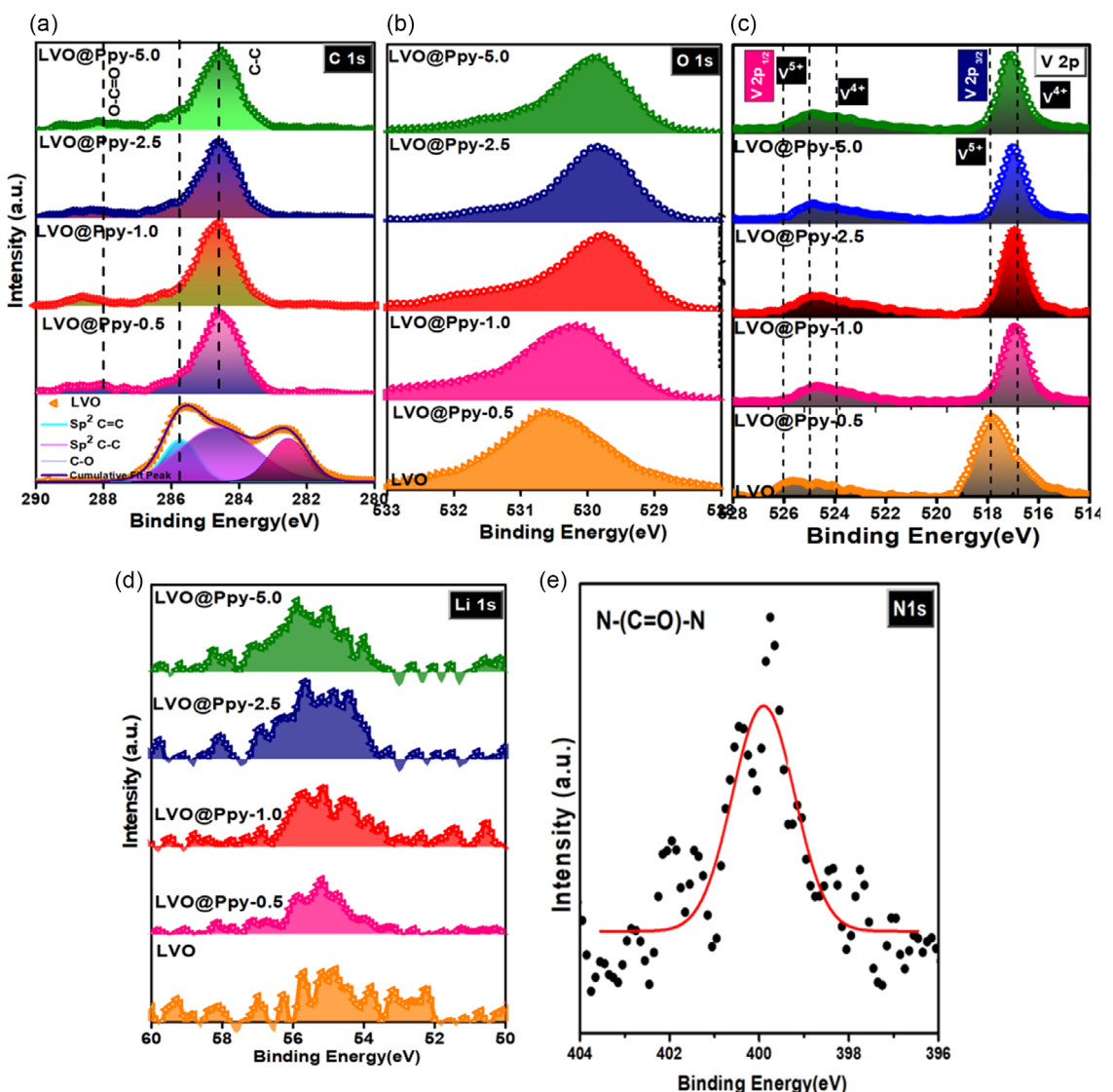


Figure 4. XPS high resolution spectra of LVO and LVO@Ppy samples: a) C 1s, b) O 1s, c) V 2p, d) Li 1s, and e) N 1s of LVO@Ppy-5.0.

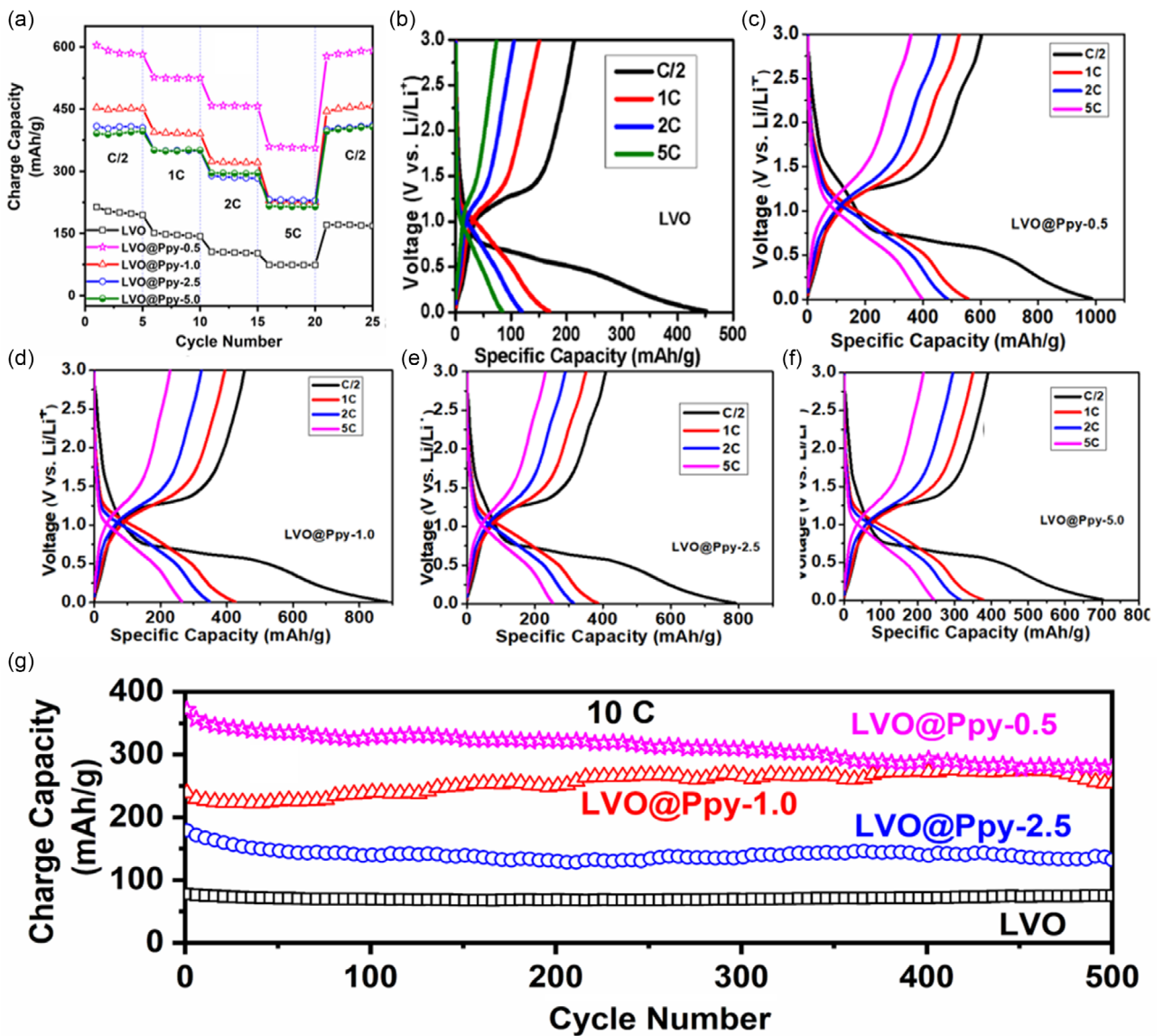


Figure 5. a) Rate performance of LVO and LVO@Ppy samples. b–f) Charge–discharge profiles of LVO, LVO@Ppy-0.5, LVO@Ppy-1.0, LVO@Ppy-2.5, and LVO@Ppy-5.0. g) Cycling data of pristine and Ppy coated LVO electrodes at 10C.

97% of the capacity retained at this current, similar to the value observed prior to the high-current testing. The result shows Ppy coating enhances the capacity of the anode, this enhancement in capacity could be attributed to the optimal Ppy layer, which provides enhanced electrical conductivity and ion diffusivity. The solid–electrolyte interface (SEI) layer in the pristine LVO anode could lead to an increased charge transfer resistance at the LVO/electrolyte interface, leading to poor electrical conductivity and reduced lithium-ion diffusion, which in turn impairs rate performance. In the LVO@Ppy anode, the Ppy layer acts as an electronic conductive layer between the electrode and the electrolyte, thereby improving rate performance. By taking into account that the theoretical specific capacity of Ppy (72 mAh g^{-1} ^[31]) is lower than that of LVO (397 mAh g^{-1}), the thin Ppy layer on the outer surface of LVO contributes less to the overall capacity. Therefore, it can be concluded that while the

capacitance of Ppy does not significantly enhance the total capacity, its electronic conductive properties positively impact the overall performance of the LVO anode.

Figure 5b shows charging and discharging behavior of bare LVO at different C rate, during the first cycle at C/2 of, the pristine-LVO anode exhibited an ICE of 47%. After this cycle the anode showed Coulombic efficiency (CE) ranging from 85% to 90% for as C rating increased from 1C to 5C. This suggests that a substantial portion of the Li⁺ ions used in forming the SEI during the first charge cycle are irreversibly inserted, making their extraction challenging. Figure 5c–f shows charging and discharging behavior of LVO@Ppy samples at different C rate. These samples are showing a slightly higher ICE 61% for LVO@Ppy-0.5 at C/2 rate. These results show further investigation is required to enhance the ICE of LVO and LVO@Ppy samples. Notably, the LVO@Ppy-0.5 anode achieved a maximum reversible charging capacity

of 605 mAh g⁻¹, which is nearly three times the capacity of Pristine-LVO. The results indicate that the Ppy coating improves capacity, with the LVO@Ppy-0.5 sample demonstrating the best performance among the polymer-coated variants. However, FESEM analysis (Figure S3, Supporting Information) reveals that the dense Ppy coating on LVO in the LVO@Ppy-5 sample results in reduced capacity. This suggests that achieving an optimal layer thickness is essential for maximizing capacity. Figure 5g demonstrates the cycling performance of the pristine-LVO and LVO@Ppy samples at 10C. The pristine LVO exhibited a charge capacity that stabilized with a CE of 98% and a reversible capacity of 65 mAh g⁻¹ at 10C, which was maintained over 500 cycles. In contrast, the LVO@Ppy-0.5 sample demonstrated a significantly higher capacity of 328 mAh g⁻¹ at 10C. Notably, LVO@Ppy-0.5 shows 78% capacity retention even after 500 cycles. A small increase in LVO@Ppy-1.0 cell could be due to gradual activation of interface active sites that leads to pseudocapacitive Li-ion storage. As a wide bandgap material, LVO has low intrinsic electronic conductivity, leading to polarization and poor rate performance. However, the results show that the conductive Ppy coating elevates electronic conductivity, allowing the LVO@Ppy anodes to exhibit lower polarization and improved reaction kinetics compared to the pristine LVO. To assess the ICE and the consistency of the prelithiation process, multiple cells were fabricated and analyzed. The open-circuit voltage (OCV) measurements yielded an average value of 1.1 ± 0.05 V. The pristine (without prelithiation) half-cell OCV is ≈3.0 V, the significantly lower value of OCV indicates a highly prelithiated state of the LVO@Ppy-0.5 anode. The charge–discharge profile (Figure S7a, Supporting Information) reveals a substantial improvement in ICE, rising from 61% for the LVO@Ppy-0.5 to 87% after prelithiation at a C/2 rate. Figure S7b, Supporting Information, presents the cycling performance and CE of the prelithiated LVO@Ppy-0.5 electrode at a 1C rate over 100 cycles, demonstrating enhanced stability and sustained CE throughout the cycling process. These findings underscore the importance of optimizing parameters such as immersion time and lithium concentration to precisely control lithium distribution and prelithiation depth, thereby enhancing the overall performance of lithium-ion batteries.

Figure S6a,b, Supporting Information, presents the cyclic voltammetric (CV) curves of bare LVO and LVO@Ppy-0.5 anodes recorded within the voltage window of 0–3.0 V at scan rates ranging from 0.5 to 25 mV s⁻¹. In the first cathodic scan of bare LVO, a distinct reduction peak appears at ≈0.33 V, which is attributed to the formation of the SEI layer along with Li⁺ intercalation. From the second cycle onward, this reduction peak shifts to ≈0.49 V, corresponding to the activation of Li₃VO₄. This behavior is also reflected in the charge–discharge profile, where a lithiation plateau is observed at ≈0.5 V (Figure 5b). For the LVO@Ppy-0.5 electrode, two cathodic peaks are observed at ≈0.33 and ≈1.7 V (Figure 5a). The additional peak at ≈1.7 V originates from the redox contribution of the polypyrrole coating. Correspondingly, the charge–discharge curves exhibit two lithiation plateaus initiating at ≈1.6 V and ≈0.7 V (Figure 5c), confirming a two stage lithiation process in Ppy-coated LVO. In both bare LVO and LVO@Ppy-0.5 electrodes, the initial reduction peak at ≈0.33 V

shifts to ≈0.49 V from the second cycle onward, further confirming SEI formation. Quantitatively, the reduction current for bare LVO reaches ≈676 mA g⁻¹, whereas the LVO@Ppy-0.5 electrode delivers a much higher current of ≈1200 mA g⁻¹ at a scan rate of 0.2 mV s⁻¹, highlighting its superior lithiation capacity. During the anodic scan, both electrodes display a dominant oxidation peak centered at ≈1.3 V. Additionally, the LVO@Ppy-0.5 electrode shows a secondary oxidation peak at ≈2.5 V, suggesting additional redox activity contributed by the polypyrrole layer. The charge profile reveals a delithiation plateau at ≈1.3 V, aligning with the oxidation peak for both electrodes, while a minor plateau at ≈2.5 V is observed only for the LVO@Ppy-0.5 electrode (Figure 5c). Interestingly, with increasing Ppy coating thickness (LVO@Ppy-1.0, LVO@Ppy-2.5, LVO@Ppy-5.0), the 2.5 V plateau in the GCD profiles, gradually diminishes and the overall capacity decreases, confirming that an optimal conformal coating is crucial to maximize the anode's performance. It is also noteworthy that at low scan rates (of the CV), the capacity is primarily governed by diffusion processes, whereas at higher scan rates, contributions from capacitive storage become significant due to the large surface area of the LVO@Ppy composite. At low sweep rates, the total stored charge is high, indicating that full storage is not achieved at higher rates due to kinetic limitations associated with Li⁺ diffusion. The integrated area under the CV curves thus represents the total stored charge, arising from both faradaic and nonfaradaic processes. The charge-storage behavior was further analyzed to distinguish the relative contributions of diffusion-controlled faradaic and surface-controlled pseudocapacitive processes. For this purpose, the relationship between peak current (*i*) and scan rate (*v*) was examined using the power-law equation.^[32]

$$i = a v^b \quad (1)$$

The logarithmic plot of current (log *i*) versus scan rate (log *v*) was constructed over a scan range of 0.5–10 mV s⁻¹ as shown in Figure S6c, Supporting Information. The slope of this linear fit provides the *b*-value, while the intercept corresponds to the constant *a*. Generally, a *b*-value near 0.5 signifies a diffusion-controlled intercalation process dominated by faradaic reactions, whereas a *b*-value close to 1.0 reflects a surface-controlled capacitive charge-storage mechanism. The calculated *b*-value for pristine LVO (0.46) is close to 0.5, indicating a diffusion-controlled intercalation process, whereas LVO@Ppy-0.5 exhibits a higher *b*-value of 0.65, signifying an increased capacitive contribution after Ppy modification. Further analysis using Dunn's method (Figure S6d, Supporting Information) confirms that the capacitive contribution dominates at higher scan rates. To quantitatively distinguish these contributions, the dependence of current on sweep rate was analyzed.^[33] At a fixed potential, the total current can be expressed as

$$i(v) = k_1 v + k_2 v^{1/2} \quad (2)$$

The terms *k*₁*v* and *k*₂*v*^{1/2} correspond to the current contributions from the surface capacitive effects and the diffusion-controlled intercalation process, respectively. The percentage contributions of pseudocapacitive-controlled and diffusion-controlled processes

of LVO and LVO@Ppy-0.5 respectively at different scan rates is given in Figure S6e,f, Supporting Information. The capacitive contribution for LVO gradually increases from $\approx 38\%$ at 0.5 mV s^{-1} to $\approx 74\%$ at 10 mV s^{-1} , whereas LVO@Ppy-0.5 shows $56\%-85\%$ increase for same scan rates. This enhancement is attributed to the synergistic effect of the conductive Ppy layer, which facilitates surface redox reactions and shortens the Li^+ diffusion path. These results demonstrate that the polypyrrole coating enhances fast surface capacitive lithiation while simultaneously improving the overall electrochemical kinetics of the electrode. near-surface electrochemical reactions and achieve fast electrons and ions transport kinetics. The highly conductive and large-surface-area Ppy layer facilitates charge transfer and Li^+ storage, thereby improving the overall capacity.

EIS was conducted to understand the electrochemical behavior, as shown in **Figure 6**. The bare LVO and LVO@Ppy-0.5 cells were analyzed under various states of charge and discharge. The high-frequency semicircle is associated with the resistance of the surface passivation layer (SEI), while the medium-frequency semicircle represents the resistance encountered during charge

transfer at the electrode/electrolyte interface.^[34] Both samples showed only a single semicircle, indicating that the impedance response is primarily influenced by the resistance of the SEI layer (R_{SEI}). Under OCV conditions, both samples exhibited comparable R_{SEI} values of $\approx 96-98 \Omega$. Upon discharging from OCV to 0.5 V, the resistance of bare LVO increased to 152Ω (Figure 6a), indicating the growth of a thicker SEI layer on the LVO surface. LVO has Li^+ intercalation potential between 0.5 and 1.0 V versus Li^+/Li . During discharge at 0.5 V, maximum Li^+ intercalation occurs, causing structural distortion in LVO. This creates new electrode/electrolyte interfaces and thickens the SEI layer, causing an increase in resistance. At the end of discharge (0.01 V), a slight reduction in R_{SEI} 125Ω was observed. During the charging process, delithiation induces the dissolution or degradation of the SEI layer, driven by Li^+ deintercalation from the LVO anode, which causes significant volume changes. Consequently, R_{SEI} decreases to 41Ω at 1.5 V and reaches a minimum of 37Ω by the end of the charging at 3.0 V. A similar trend was observed for the LVO@Ppy-0.5 electrode, though with a more pronounced

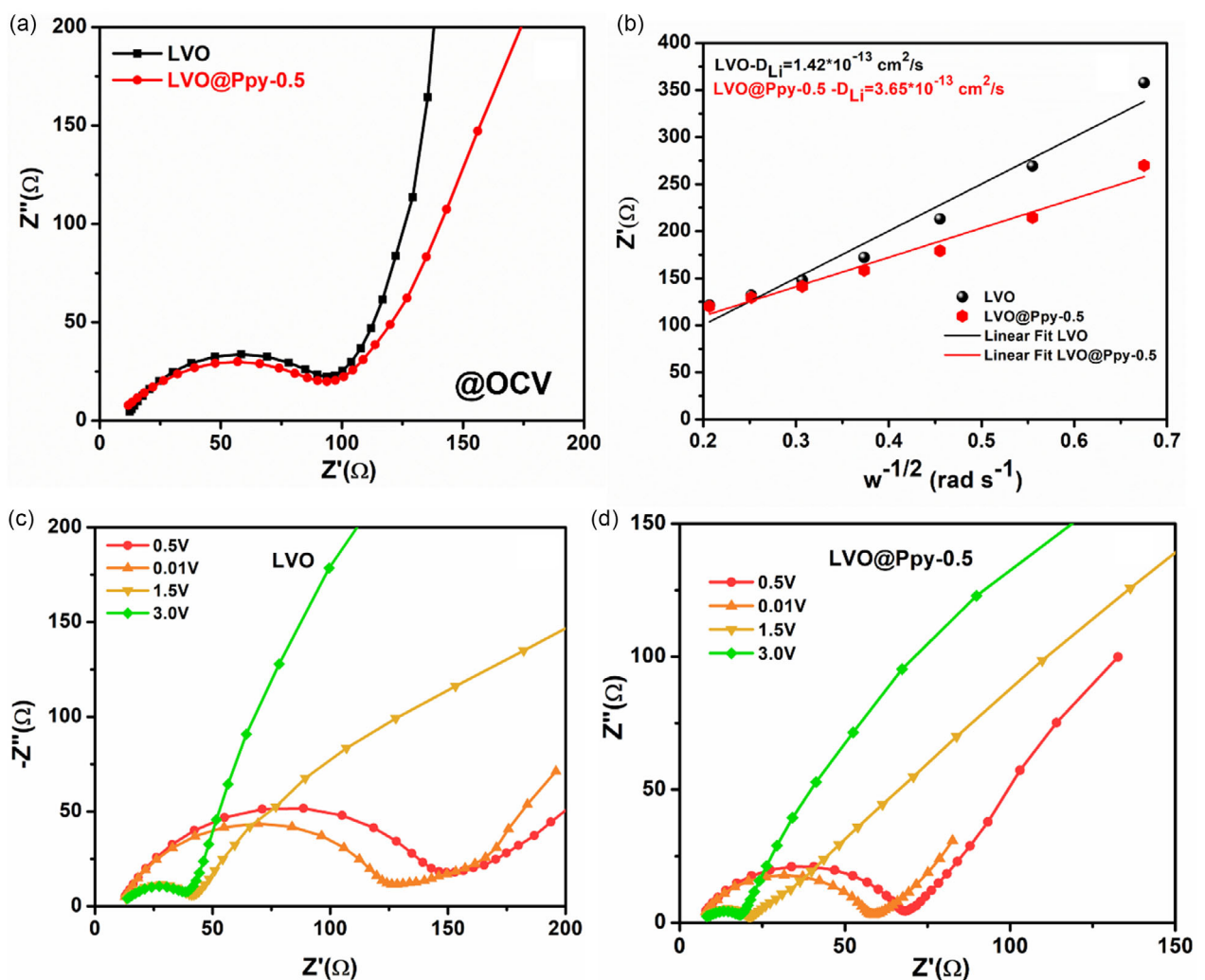


Figure 6. Nyquist plot of the a) LVO and b) LVO@Ppy-0.5 at OCV condition. (b) Relationship between Z' and $\omega^{-1/2}$ in the low-frequency region of LVO and LVO@Ppy-0.5. c,d) Nyquist plot of LVO and LVO@Ppy-0.5 at different states of charge.

reduction in R_{SEI} values. LVO@Ppy-0.5 showed 58 Ω at the end of discharge (0.01 V), and 18 Ω at the end of charging (3 V). Figure 6b displays the relationship between Z' and $\omega^{-1/2}$ at OCV condition for both LVO and LVO@Ppy-0.5 electrodes and calculated Li-ion diffusivity values by the equation given below.^[35]

$$D_{Li^+} = R^2 T^2 / 2A^2 n^4 F^4 \sigma_w^2 C^2 \quad (3)$$

where, the R is universal gas constant 8.314 J K⁻¹ mol⁻¹, T is temperature in Kelvin, A is electrode surface area, n is number of Li⁺ ions, F is faradays constant 96,485 C mol⁻¹, the slope of the curve σ_w and C concentration of the electrolyte. Similar analysis for LVO@Ppy-1.0 electrode as well and the summary of diffusivity values for all three electrodes are displayed in Table S3, Supporting Information. It is observed that the diffusivity values are maximized at the end of discharge (compared to OCV and at the end-of-charge) for all three electrodes analyzed. The lowest value was of the order of 10⁻¹³ cm² s⁻¹ while the maximum value was few 1000 times higher for the LVO@Ppy-0.5 electrode at the end-of-discharge. It is obvious from the results that LVO@Ppy-0.5 exhibit the best diffusivity value consistent with the electrochemical performances discussed earlier. The conformal Ppy coating on LVO permits electrolyte diffusion and interaction with LVO, reducing the growth of an insulating interfacial layer, significantly enhancing the electrochemical performance of the LVO@Ppy electrode by

lowering interfacial resistance and improving charge transfer kinetics. These findings suggest that the optimal thickness Ppy-coated LVO anode can provide improved cycling stability, structural integrity, and charge transfer kinetics, representing five-fold enhancement in capacity at the highest rate investigated.

Figure 7 and 8a-f shows the ex situ XPS spectra of LVO and LVO@Ppy-0.5 at pristine (uncycled state), end of first discharge to 0.01 V and end of first cycle 0.01–3.0 V for both the sample stacked bottom to top as described in figure legends. From the C 1s of the LVO and LVO@Ppy-0.5 electrodes, it is evident that both samples display characteristic peaks at 284.6 eV, corresponding to the C–C bond in carbon, and 291.1 eV, attributed to the CF₂^[36–38] groups of PVDF. An additional peak at 285.0 eV^[39] (C–O) is observed under pristine, charged, and discharged conditions, indicating the presence of carbon species bonded to oxygen, which can be ascribed to surface functional groups in the carbon nanotube. Upon charging, this C–C peak shifts slightly toward higher binding energy, which can be attributed to the formation of the SEI layer. During charge, a new peak emerges at 283.8 eV (C–Metal) could be due to C–Li and the intensity of this peak is less in LVO@Ppy-0.5 sample.

Figure 7b presents the O 1s spectrum of pristine LVO and LVO@Ppy-0.5 electrodes, showing a main peak at 530.0 eV corresponding to the V–O bond. After electrochemical cycling (charging and discharging), V–O peak intensity decreases due to SEI layer developed on the surface and new O 1s components

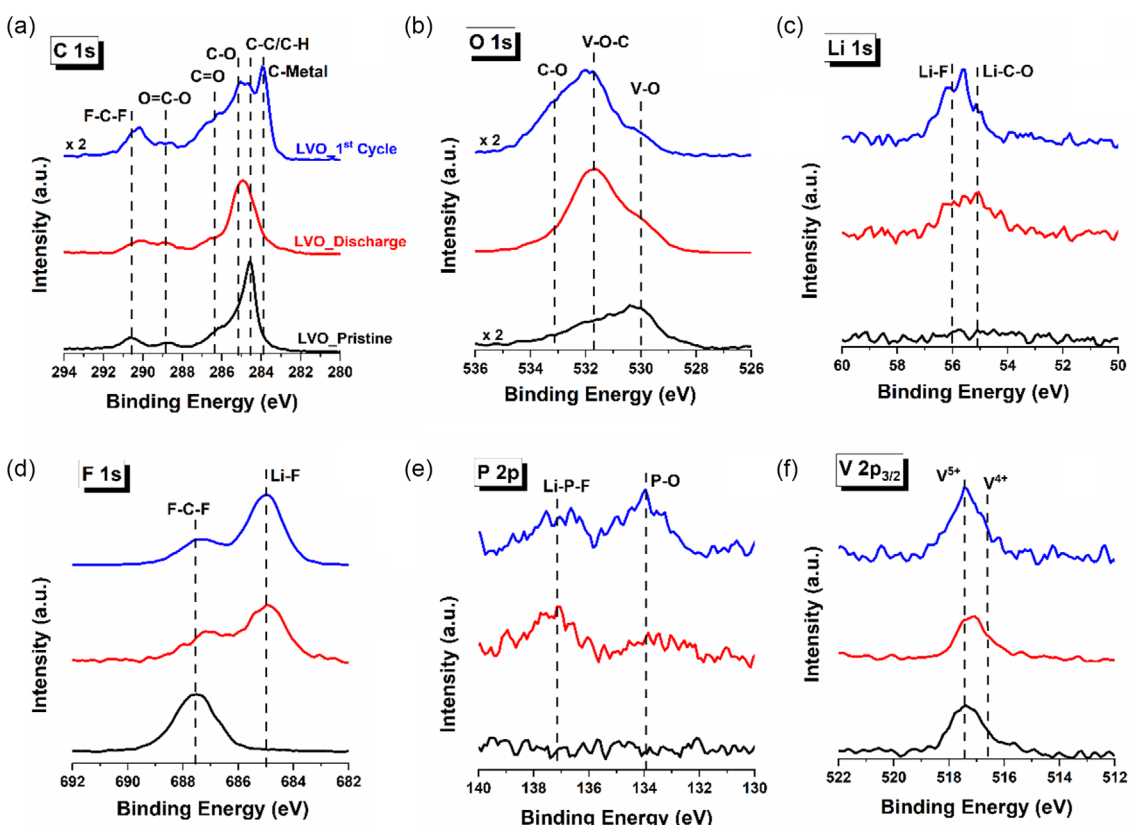


Figure 7. XPS spectra of the pristine LVO anode at different electrochemical states: pristine LVO (uncycled) anode, discharged (3.0–0.01 V), and first charged (0.01–3.0 V). a) C 1s, b) O 1s, c) Li 1s, d) F 1s, e) P 2p, and f) V 2p_{3/2} spectra.

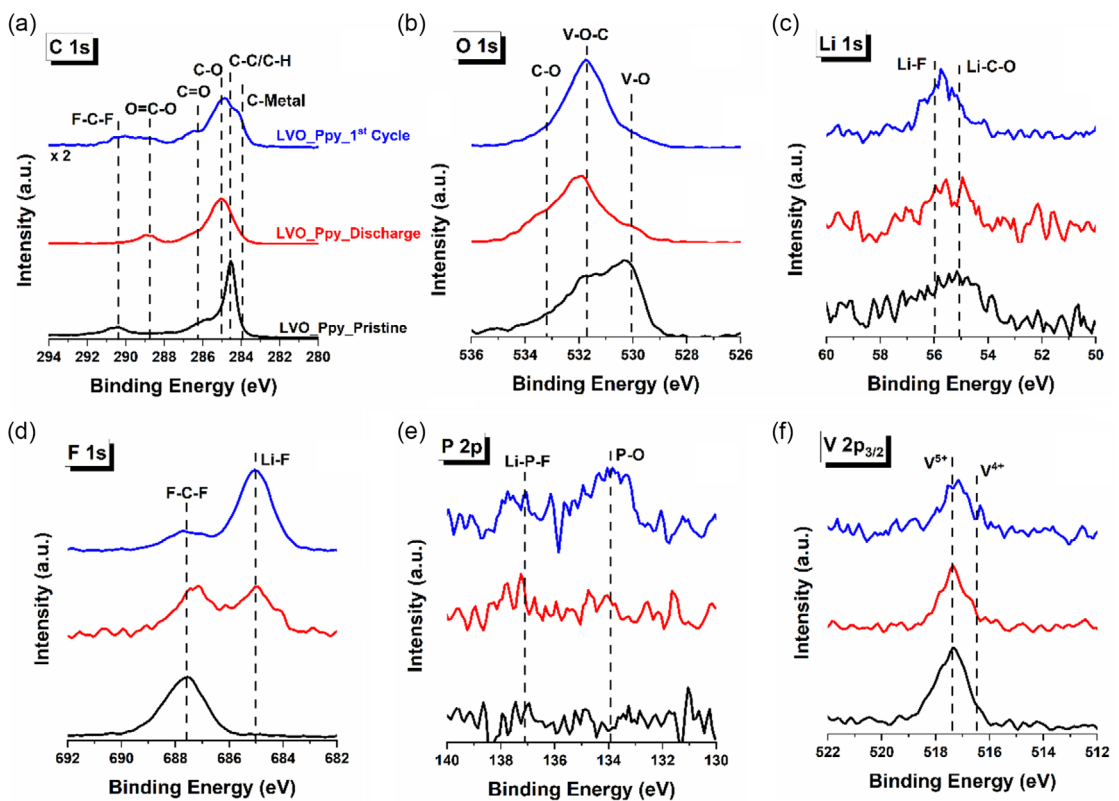


Figure 8. XPS spectra of the LVO@Ppy-0.5 anode at different electrochemical states: pristine LVO (uncycled) anode, discharged (3.0–0.01 V), and first charged (0.01–3.0 V). a) C 1s, b) O 1s, c) Li 1s, d) F 1s, e) P 2p, and f) V 2p_{3/2} spectra.

appear in the 531–534 eV region, which are associated with SEI-related species such as LiOH and Li₂CO₃ (BE ≈ 531.8 eV),^[40,41] formed by the decomposition of the organic solvent DMC (BE ≈ 532–534 eV).^[42,43] Figure 7c shows the Li 1s spectrum, where the cycled electrode exhibits peaks at 56 and 55 eV, corresponding to Li-F and Li-carbonate species, respectively, which can be ascribed to the decomposition of LiPF₆. Figure 7d and 8d displays the F 1s spectra, showing a prominent peak at 687.5 eV arising from the CF₂ groups in PVDF, while an additional peak appearing at 685 eV after cycling is attributed to LiF, a decomposition product of LiPF₆, indicating electrolyte degradation and SEI layer formation during electrochemical cycling. The P 2p spectrum displays low intensity peak at 137 eV^[43] in Figure 7e and 8e, corresponding to Li–P–F bond confirms it and another low intensity peak at 133.7 eV corresponding to P–O bond.^[43] Both in LVO and in LVO@Ppy-0.5 sample, P–O bond appears in charging cycle this corresponds to phosphate species forming in the SEI. The charging and discharging cycles confirm the formation and stability of the SEI layer. Figure 7 and 8f shows, the V 2p_{3/2} spectrum shows a distinct peak at 517.3 eV,^[30] characteristic of V⁵⁺ in Li₃VO₄, and a secondary peak at 516.5 eV, indicating partial reduction to V⁴⁺ indicating the lithium interaction into Li_{3+x}VO₄ during discharging cycle. The XPS analysis clearly demonstrates that the formation of the SEI layer substantially modifies the surface chemistry of the anode. The SEI introduces new peaks corresponding to inorganic lithium compounds (such as Li₂CO₃, LiF, and Li₂O_x), induces binding energy shifts, and reduces the intensity of the

underlying electrode signals. These spectral changes confirm the development of a chemically complex SEI layer that passivates and stabilizes the electrode surface during cycling. The polypyrrole coating, in particular, acts as a protective barrier, effectively reducing electrolyte decomposition and serving as an artificial SEI layer by minimizing the direct exposure of the active material to the electrolyte and thereby suppressing excessive SEI growth.

In the C 1s region, pristine LVO exhibits a persistent F–C–F signature attributable to PVDF across the uncycled, first-discharge and first-charge states, consistent with exposed binder. From C 1s spectra, for LVO@Ppy the F–C–F intensity is substantially reduced after first discharge. The F 1s spectra contain components assignable to both PVDF (F–C–F) and electrolyte-decomposition products (LiF/PF₆ derivatives), and the PPy-coated electrode displays relatively stronger F-derived intensity in the uncycled state. At first discharge, the LVO@Ppy-0.5 has similar intensity for LiF and F–C–F. After cycling, LiF becomes the dominant F species, indicating LiPF₆ decomposition during lithiation and accumulation of insoluble LiF on the surface. Pristine O 1s spectra show a clear lattice V–O contribution for both samples, with the PPy-coated pristine electrode exhibiting a relatively larger V–O fraction than the uncoated sample. The V–O and V–O–C bond is more prominent in coated sample with mere C–O present in all state. V–O and C–O species are more in all the states of pristine LVO. Upon cycling, carbonate-type features (C–O and C=O) increase markedly on bare LVO especially after

the first cycle, whereas, this increase is not so prominent for LVO@Ppy. No appreciable Li signal is detected at the immediate surface of pristine bare LVO, as expected; after first charge on bare LVO both Li—C—O (organic SEI) and LiF signals appear with comparable intensity, and after the first cycle LiF becomes the dominant Li environment, consistent with progressive inorganic SEI formation from LiPF₆ decomposition. Notably, the Li 1s spectra of LVO@Ppy indicate that the coated surface exhibit minor concentration of LiF and Li—C—O. P 2p signals (P—O and Li—P—F) are absent in uncycled electrodes and appear only after first discharge and first charge for both bare and coated samples, confirming that P-containing decomposition products arise from electrochemical PF₆ degradation and become part of the interfacial layer. Across all ex situ surface spectra, the V 2p region remains dominated by V⁵⁺ and V⁴⁺. In summary, in vapor-phase polymerization of polypyrrole (Ppy) on LVO, FeCl₃ serves a dual role as both oxidant and dopant. The LVO substrate is first soaked in FeCl₃ solution and then exposed to pyrrole vapor, where FeCl₃ oxidizes the pyrrole monomers, initiating their polymerization into conductive PPy. During this process, FeCl₃ is reduced to Fe²⁺, while chloride ions (Cl⁻) act as dopants, incorporating into the PPy backbone and generating mobile charge carriers that enhance its electrical conductivity.^[44] Therefore, the residual FeCl₃ species in the LVO@Ppy composite act as dopants that enhance conductivity and may contribute positively to the overall electrochemical performance. This study presents a systematic thickness-dependent study (LVO@Ppy-0.5, LVO@Ppy-1.0, LVO@Ppy-5.0) that reveals the critical role of polymer layer thickness in determining electrochemical performance. These findings extend beyond existing reports by providing new insights into how coating thickness influences lithium-ion diffusion, electronic conductivity, and interfacial area, thereby establishing clear design principles for polymer-coated oxide anodes.

4. Conclusions

In this study, we showcased the hydrothermal synthesis of crystalline layered LVO-based anodes for Li-ion batteries, achieving improved capacity and cycling performance with the conductive Ppy coating. Layered structure of LVO facilitates better electrolyte penetration, shortened diffusion distances for lithium ions, and increased the number of charge transfer reaction sites. Surface morphology analysis and EIS reveal that a conductive layer coating on the LVO also reduced its charge transfer resistance, further improving rate performance. The amount of Ppy deposited on LVO increased with polymerization time. LVO@Ppy-0.5 initially exhibited minimal surface coverage, but as polymerization time increased, the Ppy layer on LVO became thicker and denser. The conformal coating of Ppy coating offers several benefits for the LVO electrode material. First, it provides a more conductive pathway for electrons, enabling faster Li⁺ ion migration, which is essential for achieving high-rate performance. The Ppy layer on LVO not only improved capacity but also improves the rate performance. Without the Ppy coating, LVO directly exposed to the electrolyte results in an extensive LVO-electrolyte interface,

generating a substantial amount of SEI during the initial lithiation process, which acts as an insulating layer, hindering charge transfer. However, when a thin Ppy layer is formed on LVO, a portion of the electrolyte can still penetrate through the Ppy layer and interact with LVO, reducing the growth of an insulating SEI layer. However, when the Ppy layer becomes too thick, it inhibits the electrolyte from accessing the LVO layer, leading to a reduction in capacity. This reduction likely occurs because the thick Ppy layer obstructs lithium-ion diffusion and decreases the active LVO content that interacts with the electrolyte. Ex situ XPS analysis demonstrates that cycling induces the formation of a chemically complex SEI layer on both LVO and the polypyrrole-coated LVO, containing Li-based inorganic compounds and electrolyte decomposition products that stabilize the electrode surface. The polypyrrole coating reduces excessive SEI formation, suppresses electrolyte decomposition, and preserves the active material. The quantitative diffusivity values are consistent with these observations and the electrochemical performance of LVO@Ppy-0.5. LVO@Ppy-0.5, with an optimal Ppy thickness, allows lithium ions to diffuse freely into the LVO, while the Ppy functions as an efficient channel for electron transfer. In contrast, a thicker Ppy layer not only obstructs lithium-ion diffusion into the LVO layer and increasing charge transfer resistance thereby diminishing overall performance. Therefore, a conformal thin Ppy layer and chemical prelithiation that can balance all these factors to maximize the performance. In this case, the LVO@Ppy-0.5 sample, featuring an optimal conformal PPy coating of ≈4 nm and subjected to 1 min of chemical prelithiation, exhibits a significant enhancement in both capacity and ICE of 87%.

Acknowledgements

The authors thank Amrita Vishwa Vidyapeetham for the financial support (Ref: K-ACNS-23-707) and fellowship for DSB.

Conflict of Interest

The authors declare no conflict of interest.

Author Contributions

Mini Pothanadu Antony: data curation (lead); formal analysis (lead); investigation (lead); writing—original draft (lead). **Dona Susan Baji:** data curation (equal); investigation (supporting); writing—review and editing (supporting). **Shantikumar Nair:** conceptualization (supporting); resources (lead); writing—review and editing (supporting). **Dhamodaran Santhanagopalan:** conceptualization (lead); project administration (lead); supervision (lead); writing—review and editing (equal).

Data Availability Statement

The data that support the findings of this study are available from the corresponding author upon reasonable request.

Keywords: anode · conducting polymer · conformal coating
Li-ion battery · Li₃VO₄ · polypyrrole

- [1] D. Gayen, R. Chatterjee, S. Roy, *Int. J. Environ. Sci. Technol.* **2024**, *21*, 5285.
- [2] Y. Chen, Y. Kang, Y. Zhao, L. Wang, J. Liu, Y. Li, Z. Liang, *J. Energy Chem.* **2021**, *59*, 83.
- [3] M. Şen, M. Özcan, Y. R. Eker, *Next Sustainability* **2024**, *3*, 100036.
- [4] P. U. Nzereogu, A. D. Omah, F. I. Ezema, E. I. Iwuoha, A. C. Nwanya, *Appl. Surface Sci. Adv.* **2022**, *9*, 100233.
- [5] M. H. Hossain, M. A. Chowdhury, N. Hossain, M. A. Islam, M. H. Mobarak, *Chem. Eng. J. Adv.* **2023**, *16*, 100569.
- [6] B. Gangaja, S. Nair, D. Santhanagopalan, *Nano-Micro Lett.* **2020**, *12*, 1.
- [7] T. F. Yi, L. J. Jiang, J. Shu, C. B. Yue, R. S. Zhu, H. B. Qiao, *J. Phys. Chem. Solids* **2010**, *71*, 1236.
- [8] A. Abouimrane, Y. Cui, Z. Chen, I. Belharouak, H. B. Yahia, H. Wu, R. Assary, L. Curtiss, K. Amine, *Nano Energy* **2016**, *27*, 196.
- [9] N. S. Shaikh, P. Kanjanaboons, V. C. Lokhande, S. Praserttham, C. D. Lokhande, J. S. Shaikh, *ChemElectroChem* **2021**, *8*, 4686.
- [10] Y. S. Hsiao, J. H. Huang, L. Y. Weng, T. H. Cheng, H. H. Chiang, C. Z. Lu, H. C. Weng, L. Thomsen, B. Cowie, W. K. Pang, Y. C. Huang, *Chem. Eng. J.* **2024**, *489*, 150973.
- [11] C. Wang, C. Pei, L. Lei, Z. Chen, D. Zhang, B. Sun, P. Li, H. Ma, Z. Shen, S. Ni, *J. Mater. Chem. A* **2025**, *13*, 5275.
- [12] M. E. A.-D. Domípablo, P. Tartaj, J. M. Amarilla, U. Amador, *Chem. Mater.* **2016**, *28*, 5643.
- [13] J. Zhou, B. Zhao, J. Song, B. Chen, X. Ma, J. Dai, X. Zhu, Y. Sun, *Chem. Eur. J.* **2017**, *23*, 16338.
- [14] G. Shao, L. Gan, Y. Ma, H. Li, T. Zhai, *J. Mater. Chem. A* **2011**, *3*, 11253.
- [15] J. Yao, X. Bai, D. Zhang, S. Yang, C. Pei, S. Ni, *J. Energy Storage* **2024**, *102*, 114193.
- [16] X. Bai, D. Li, D. Zhang, S. Yang, C. Pei, B. Sun, S. Ni, *J. Mater. Chem. A* **2023**, *11*, 12164.
- [17] S. C. Hsu, K. S. Wang, Y. T. Lin, J. H. Huang, N. J. Wu, J. L. Kang, H. C. Weng, T. Y. Liu, *Polymers* **2023**, *15*, 2502.
- [18] L. Wang, C. Zheng, J. Liang, C. Zhai, H. Liu, T. Zhai, H. Li, *Inorganic Chem. Front* **2024**, *11*, 1177.
- [19] Z. Zhang, C. Pei, D. Zhang, J. Lu, T. Li, T. Xiao, S. Ni, *ACS Appl. Mater. Interfaces* **2022**, *14*, 35854.
- [20] Y. Luo, R. Guo, T. Li, F. Li, Z. Liu, M. Zheng, B. Wang, Z. Yang, H. Luo, Y. Wan, *ChemSusChem* **2019**, *12*, 1591.
- [21] S. Martha, D. K. Mishra, in *Conducting Polymer-Based Energy Storage Materials*, (Eds: Inamuddin, R. Boddula, M. F. Ahmer, A. M. Asiri) CRC Press, USA **2019**, pp. 79, Ch. 4.
- [22] M. Zhang, J. Zhong, J. Zhu, W. Kong, Y. Wang, *J. Electroanal. Chem.* **2022**, *909*, 116155.
- [23] X. Sun, H. Zhang, L. Zhou, X. Huang, C. Yu, *Small* **2016**, *12*, 3732.
- [24] K. Varghese, D. S. Baji, S. Nair, D. Santhanagopalan, *Front. Mater. Sci.* **2022**, *16*, 220601.
- [25] R. Johnson, D. S. Baji, S. Nair, D. Santhanagopalan, *J. Ind. Eng. Chem.* **2024**, *133*, 473.
- [26] N. V. Blinova, J. Stejskal, M. Trchová, J. Prokeš, M. Omastová, *Eur. Polymer J.* **2007**, *43*, 2331.
- [27] G. Yang, B. Zhang, J. Feng, Y. Lu, Z. Wang, V. Aravindan, J. Liu, M. Srinivasan, Z. Shenabc, Y. Huang, *J. Mater. Chem. A* **2018**, *6*, 456.
- [28] M. Feng, W. Lu, Y. Zhou, R. Zhen, H. He, Y. Wang, C. Li, *Sci. Rep.* **2020**, *10*, 15370.
- [29] C. J. Cui, G. M. Wu, J. Shen, B. Zhou, Z. H. Zhang, H. Y. Yang, S. F. She, *Electrochim. Acta* **2010**, *55*, 2536.
- [30] P. B. Madambakkattil, S. Nair, D. Santhanagopalan, *ACS Appl. Energy Mater.* **2022**, *5*, 10473.
- [31] P. Novák, K. Müller, K. S. V. Santhanam, O. Haas, *Chem. Rev.* **1997**, *97*, 207.
- [32] M. Yan, D. Zhang, Q. Ouyang, X. Zhang, Y. Wang, X. Zhao, G. Li, L. Li, *Electrochim. Acta* **2003**, *470*, 143303.
- [33] J. Wang, J. Polleux, J. Lim, B. Dunn, *J. Phys. Chem. C* **2007**, *111*, 14925.
- [34] W. Choi, H. C. Shin, J. M. Kim, J. Y. Choi, W. S. Yoon, *J. Electrochem. Sci. Technol.* **2020**, *11*, 1.
- [35] D. S. Baji, K. D. Velimpampil, S. Nair, D. Santhanagopalan, *Appl. Surf. Sci.* **2025**, *708*, 163749.
- [36] Y.-C. Lu, A. N. Mansour, N. Yabuuchi, Y. S. Horn, *Chem. Mater.* **2009**, *21*, 4408.
- [37] L. C. Lopez, M. G. Buonomenna, E. Fontananova, G. Lacoviello, E. Drioli, R. d'Agostino, P. A. Favia, *Adv. Funct. Mater.* **2006**, *16*, 1417.
- [38] N. Vandencasteele, D. Merche, F. Reniers, *Surf. Interface Anal.* **2006**, *38*, 526.
- [39] Y. M. Shulga, T. C. Tien, C. C. Huang, S. C. Lo, V. E. Muradyan, N. V. Polyakova, Y. C. Ling, R. O. Loufty, A. P. Moravsky, *J. Electron Spectrosc. Relat. Phenom.* **2007**, *160*, 22.
- [40] R. Dedryvere, L. Gireaud, S. Grugéon, S. Laruelle, J.-M. Tarascon, D. Gonbeau, *J. Phys. Chem. B* **2005**, *109*, 15868.
- [41] M. Xu, W. Li, B. L. Lucht, *J. Power Sources* **2009**, *193*, 804.
- [42] R. Guo, P. Shi, X. Cheng, L. Sun, *Electrochim. Acta* **2009**, *54*, 5796.
- [43] Y. Zou, Y. Shen, Y. Wu, H. Xue, Y. Guo, G. Liu, J. Ming, *Chem. Eur. J.* **2020**, *26*, 7930.
- [44] Y. Sood, K. Singh, H. Mudila, P. E. Lokhande, L. Singh, D. Kumar, A. Kumar, M. H. Dehghani, *Heliyon* **2024**, *10*, e33643.

Manuscript received: July 30, 2025

Revised manuscript received: October 10, 2025

Version of record online: